

Article

Arsenic (III) Removal from a High-Concentration Arsenic (III) Solution by Forming Ferric Arsenite on Red Mud Surface

Dongdong He, Yuming Xiong, Li Wang, Wei Sun, Runqing Liu * and Tong Yue *

School of Minerals Processing and Bioengineering, Central South University, Changsha 410083, China; hedongdong@csu.edu.cn (D.H.); xiongyym3@mail2.sysu.edu.cn (Y.X.); li_wang@csu.edu.cn (L.W.); sunmenghu@csu.edu.cn (W.S.)

* Correspondence: 211038@csu.edu.cn (R.L.); yuetong@csu.edu.cn (T.Y.)

Received: 30 April 2020; Accepted: 23 June 2020; Published: 28 June 2020

Abstract: Arsenic (As) is considered one of the most serious inorganic pollutants, and the wastewater produced in some smelters contains a high concentration of arsenic. In this paper, we purified the high-concentration arsenic solution with red mud and Fe^{3+} synergistically. In this system, arsenite anions reacted with Fe(III) ions to form ferric arsenite, which attached on the surface of red mud particles. The generated red mud/ $\text{Fe}_{1-x}(\text{As})_x(\text{OH})_3$ showed a better sedimentation performance than the pure ferric arsenite, which is beneficial to the separation of arsenic from the solution. The red mud not only served as the carrier, but also as the alkaline agent and adsorbent for arsenic treatment. The effects of red mud dosage, dosing order, pH, and molar ratio of Fe/As on arsenic removal were investigated. The efficiency of arsenic removal increased from a pH of 2 to 6 and reached equilibrium at a pH of 7. At the Fe/As molar ratio of 3, the removal efficiency of arsenic ions with an initial concentration of 500 mg/L reached 98%. In addition, the crystal structure, chemical composition, and morphological properties of red mud and arsenic removal residues (red mud/ $\text{Fe}_{1-x}(\text{As})_x(\text{OH})_3$) were characterized by XRD, XPS, X-ray fluorescence (XRF), SEM-EDS, and Raman spectroscopy to study the mechanism of arsenic removal. The results indicated that most of the arsenic was removed from the solution by forming $\text{Fe}_{1-x}(\text{As})_x(\text{OH})_3$ precipitates on the red mud surface, while the remaining arsenic was adsorbed by the red mud and ferric hydroxide.

Keywords: arsenic removal; red mud; ferric arsenite; synergistic effect

1. Introduction

Arsenic (As) is considered one of the most serious inorganic pollutants, and the most abundant and potential inorganic carcinogen [1,2]. Consumption of arsenic-rich water causes different types of chronic disease, such as Blackfoot disease, pigmentation, keratosis, nausea, and cancer [3,4]. It has been accepted that the major source of arsenic contaminates in groundwater is geological deposits, and arsenic in the atmosphere mainly comes from geological activities. Moreover, the dissolution of arsenic-bearing sulfide minerals in nature can aggravate the hazard of acid mine drainage (AMD) [5,6]. Arsenic presents mainly in the form of arsenite AsO_3^{3-} and arsenate AsO_4^{3-} in aqueous environments and natural waters [7], while the As(III) species are much more toxic than As(V) [8,9]. The pollution of groundwater by arsenic is a serious threat to human beings all over the world. Arsenic enters the food chain, resulting in widespread distribution to entire plant and animal populations. The most common methods for arsenic removal include oxidation [10,11], coprecipitation [12,13], ion exchange [14,15], membrane filtration [16,17], and adsorption [18–20]. In addition, it has been reported that certain biotechnologies can be used to treat arsenic-contaminated water [21,22]. Among various arsenic treatment techniques, arsenic removal by forming precipitates

with ferric ions is a generally adopted method. The arsenic removal from dilute arsenite-bearing solution with the concentration of arsenic being less than 100 mg/L occurs by the adsorption of iron oxides, such as ferrihydrite, goethite, and ferric oxyhydroxide gel [23–25]. Several researchers have reported the formation of ferric arsenite in acidic solutions with high concentrations of arsenic [26]. However, it is difficult to filter ferric arsenite, due to its poor crystalline structure [23]. Red mud is a highly alkaline solid waste discharged from alumina production, and approximately 120 Mt of red mud is produced annually around the world [25]. Red mud was widely explored for its potential to remove arsenic from water. The arsenic adsorption capacity of red mud can be improved by heat or by acid treatment [27], but the related operations are complex and costly.

We have developed a technical process to treat high arsenic-bearing solutions using Fe^{3+} and red mud synergistically. In this system, arsenic removal from a high-concentration arsenic (III) solution was done by forming iron arsenite on a red mud surface. The red mud served as the carrier to improve sedimentation performance. The effects of red mud dosage, dosing order, pH, and a molar ratio of Fe/As on arsenic removal were investigated. The crystal structure, chemical composition, and morphological properties of red mud and arsenic removal residues ($\text{red mud}/\text{Fe}_{1-x}(\text{As})_x(\text{OH})_3$) were characterized by XRD, XPS, X-ray fluorescence (XRF), SEM-EDS, and Raman spectroscopy to study the mechanism of arsenic removal.

2. Materials and Methods

2.1. Experiment Material

The concentrated sulfuric acid (H_2SO_4), iron sulfate ($\text{Fe}_2(\text{SO}_4)_3$), sodium hydroxide (NaOH), and sodium arsenite (NaAsO_2) used in the experiments are of analytical grade. The red mud samples in the Bayer process were obtained from Shandong, and its XRD pattern is shown in Figure 1. Its elemental composition and percentage analysis are shown in Table 1.

It can be seen from Figure 1 that the diffraction peaks in the original red mud are consistent with the standard card PDF-NO.87-1166 of Fe_2O_3 , which shows that the iron oxide of the original red mud mainly exists in the form of Fe_2O_3 . The peaks at 18.30° and 20.28° are mainly caused by $\text{Al}(\text{OH})_3$, while the peaks at 13.92° and 24.23° are mainly contributed to by aluminosilicate.

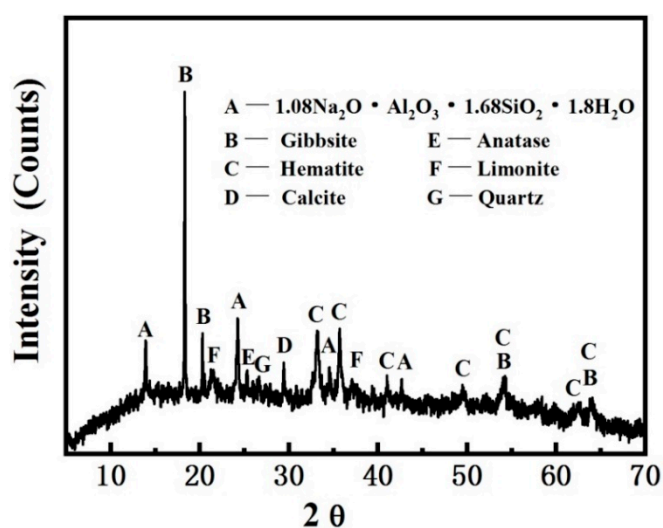


Figure 1. X-ray diffraction analysis of the original red mud.

Table 1 shows that the Na_2O content in the original red mud is 9.79%, and sodium is mainly found in complex aluminosilicates.

Table 1. Element composition and percentage content of original red mud.

Element	Al ₂ O ₃	CaO	Fe ₂ O ₃	TiO ₂	Na ₂ O	SiO ₂
Content/%	20.57	2.10	33.1	5.77	9.79	15.10

2.2. Arsenic Removal Tests

A total of 5 g/L NaAsO₂ solution and 1 mol/L NaOH solution were prepared by the analytical reagent NaAsO₂ and NaOH powder with deionized water, respectively. Arsenic solution at 500 mg/L was added into a beaker, followed by the addition of Fe³⁺ (1 g/L), red mud (0–90 g/L), and NaOH solution (1 mol/L) in different orders to study the effects of addition order on arsenic removal. The final pH was adjusted to 1–8 using different dosages of NaOH solution. After stirring at 500 rpm at 25 °C for 30 min, the solution samples were filtered and the arsenic concentrations in the filtrates were determined.

2.3. Settling Performance Test

In order to study the sedimentation performance of arsenic removal residues with different amounts of red mud, the solution in the reaction beaker was fully shaken after the reaction was complete. The solution was quickly poured into a 100 mL sedimentation column with the same model and height in order to start the sedimentation test. A suitable volume of a water sample was taken from the sampling port at the settling time of 10, 30, and 60 min, respectively, and the suspended solid concentration of each water sample was analyzed by ultraviolet-visible spectrophotometry.

2.4. Analytical Techniques

The concentrations of arsenic and iron were measured via inductively coupled plasma atomic emission spectroscopy (ICP-AES, 5110, Agilent Technologies Inc., Santa Rosa, CA, USA). The crystal structure, chemical composition, and morphological characteristics of red mud and arsenic removal residues were characterized by X-ray diffraction (XRD, SIMENS D500, Bruker, Fällanden, Switzerland), X-ray photoelectron spectroscopy (XPS, ESCALAB 250xi, Thermo Fisher Scientific, Waltham, MA, USA), X-ray fluorescence (XRF, AxiosMAX, Panalytical B.V., Almelo, The Netherlands), scanning electron microscopy energy dispersive spectroscopy (SEM-EDS, HELIOS 600i, FEI, Hillsboro, OR, USA), and Raman spectroscopy (inVia Qontor, Renishaw, London, UK), respectively. The water sample obtained from the sedimentation test was tested by an ultraviolet-visible spectrophotometer (UV2600, Shimadzu, Kyoto, Japan).

3. Results and Discussion

3.1. Arsenic Removal Experiments

The dosing sequence experiment results are shown in Table 2. It shows that the efficiency of arsenic removal when trivalent iron is added first is better than the efficiency of arsenic removal when an alkaline reagent is added first. The pH adjustment caused by red mud or by NaOH has no significant effect on arsenic removal. The main reason for arsenic removal is the formation of ferric arsenite precipitation, rather than the adsorption of red mud for high concentration arsenic solution. From reaction Equations (1) to (2), it can be seen that in the acid environment, when Fe³⁺ is added first, and then the alkaline material is added, Fe³⁺ preferentially forms the ferric arsenite with the arsenite anion. However, in the reaction vessel where the alkaline substance was added first, the solution contains abundant hydroxyl ions. In this condition, the hydroxyl ions compete with the arsenite ions to react with the subsequently added Fe³⁺ to form a Fe(OH)₃ colloid, inhibiting the formation of ferric arsenite [28,29]. In addition, adding red mud or NaOH to adjust pH has almost no influence on arsenic removal. The adsorption ability of red mud in the arsenic removal process was probably not reflected, which could be due to the fact that arsenic is removed mainly by forming ferric arsenite through precipitation instead of through adsorption. In the experiments of Fe³⁺ + NaOH

and Fe^{3+} + Red mud, the alkaline content needed in order to adjust the pH to 7 was explored at the Fe/As molar ratio of 2. The amount of iron is already very low compared to the industrially used $\text{Fe}(\text{OH})_3$ colloids for water treatment due to the forming of the ferric arsenic. To adjust the pH of 100 mL arsenic-bearing solution (500 mg/L), the required amount of NaOH and red mud were 9.8 mL and 18 g, respectively. This red mud dosage is not of application significance, because in the process of river water and surface water treatment, adding more red mud would also cause greater pollution of the water. Therefore, in the subsequent experiments, when we explored the combination of red mud and NaOH to adjust pH, the adsorption performance of red mud during the adjustment of pH was retained.



Table 2. Effect of reagent addition sequence on arsenic removal.

Agent Addition Sequence	Fe^{3+} + NaOH	Fe^{3+} + Red Mud	Red Mud + Fe^{3+}	NaOH + Fe^{3+}
As concentration after reaction (mg/L)	11.98 ± 0.23	13.14 ± 0.31	29.79 ± 0.82	49.54 ± 1.52
Arsenic removal (%)	97.60%	97.37%	94.04%	90.09%

In order to study the effect of red mud addition on arsenic removal, the following experiment was performed. A total of 1 g/L Fe^{3+} was added into 100 mL arsenic-bearing solution (500 mg/L), followed by adding 0, 20, 40, 60, 80, and 90 g/L red mud, respectively. Then, NaOH was added to adjust the pH at 7. The results shown in Figure 2 indicate that the red mud addition has great influence on arsenic removal. The arsenic concentration after reaction in particular declines from 68.95 to 14.94 mg/L with the addition of red mud from 0 to 90 g/L, and the arsenic removal efficiency increases from 84.21% to 97.01%. The main reason is that a large amount of red mud contributes to the adsorption of arsenic.

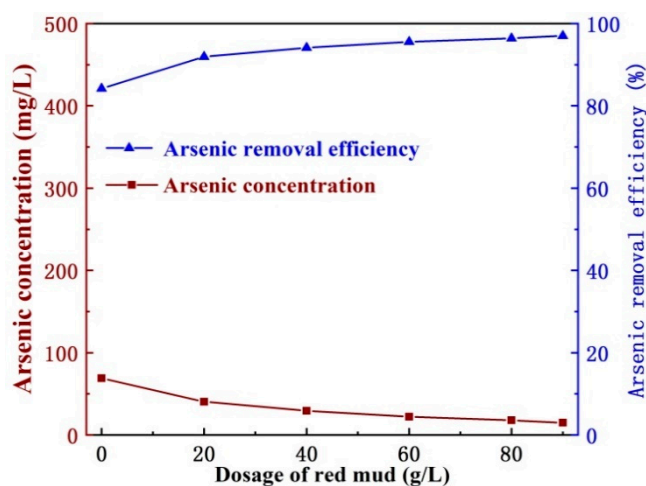


Figure 2. Effect of red mud dosage on arsenic removal.

In order to study the effect of the pH of the arsenic-containing solution on arsenic removal, the following experiment was performed. A total of 4.55 g of iron sulfate powder and 1 g of the original red mud were added to a beaker containing 1 L of 500 mg/L arsenic solution, followed by adding 1 mol/L NaOH solution. The effect of pH on arsenic removal is shown in Figure 3. When the additional amount of NaOH was less than 12 mL (pH < 2), the arsenic removal effect was very poor, and the arsenic concentration in the solution remained almost unchanged; when 18–46 mL of NaOH was added, the pH changed from 1.46 to 6.26, and the arsenic removal efficiency was greatly improved with the increase of the NaOH amount. Among them, in the pH range of 2 to 6, the arsenic removal

became very fast, which should be attributed to the increase of arsenite anions in solution with increasing the pH, achieving a high supersaturation of ferric arsenite [30]. When pH reached 7, the arsenic removal was complete.

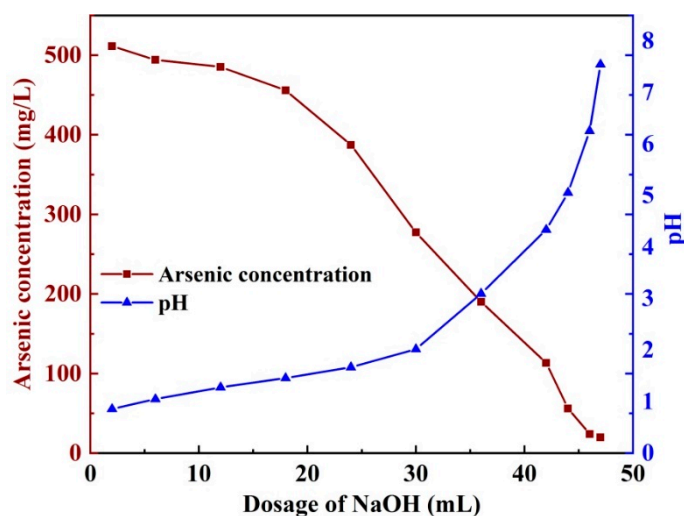


Figure 3. Effect of NaOH dosage on arsenic removal.

The arsenic removal was affected by both the initial arsenic concentration and the molar ratio of Fe/As. In order to study the effect of the initial arsenic concentration on arsenic removal, the following experiment was conducted: 4.55 g of iron sulfate powder and 1 g of the original red mud were added to a beaker containing 1 L of the prepared arsenic solution. The concentration of the prepared arsenic solution was 100, 300, 500, 600, 800, and 1000 mg/L, while the molar ratio of Fe/As was 10, 3.3, 2, 1.67, 1.25, and 1.0, respectively. The NaOH was added to adjust the pH to 7. Results are shown in Figure 4.

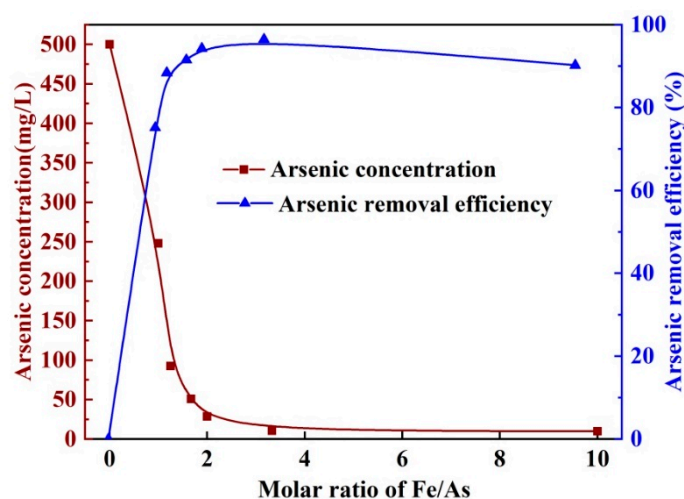


Figure 4. The arsenic removal of red mud/ $\text{Fe}_{1-x}(\text{As})_x(\text{OH})_3$ at different Fe/As molar ratio.

Figure 4 shows that when the molar ratio of Fe/As is below 3, the arsenic removal efficiency increases with the increasing of the molar ratio of Fe/As. When the molar ratio of Fe/As is more than 3, the increase of iron does not promote arsenic removal efficiency. The main reason is that the arsenic can be removed completely by forming ferric arsenite precipitates with an Fe/As molar ratio of more than 3:1 [31,32].

3.2. Sedimentation Performance

In order to explore the possibility of further industrial application of the red mud/ $\text{Fe}_{1-x}(\text{As})_x(\text{OH})_3$, the sedimentation performance of arsenic removal residues was studied. We evaluated the sedimentation performance of the arsenic removal residues by measuring the turbidity of the supernatant after the reaction for a certain period of time. The turbidity of the sample was inferred by measuring the absorption value of the supernatant with ultraviolet spectrophotometry. The greater the absorption intensity, the higher the turbidity of the supernatant, as the more solid matter there was in it. The supernatant of the reaction system was analyzed via UV spectroscopy with 185–700 nm wavelength, as shown in Figure 5.

According to Figure 5, it is preliminarily determined that with the increase of sedimentation time, the supernatant becomes clearer, and the absorption value of light gradually decreases. In Figure 5, the peak value and peak area of the absorption intensity were reduced. In addition, the sedimentation performance of the system with 0.1 g of red mud was always better than that of the sample without red mud at the same time, indicating that the red mud improved the sedimentation performance of arsenic removal residues. The formation and aggregation of the ferric arsenite on the surface of the red mud particles is significantly beneficial for enhancing the sedimentation performance of the arsenic removal residues. Additionally, the little amount of residual flocculant in red mud may played a certain role in sedimentation performance. This solved the problem of settlement difficulties when colloidal ferric arsenite is formed. In summary, the red mud/ $\text{Fe}_{1-x}(\text{As})_x(\text{OH})_3$ not only had a good arsenic removal effect but also showed good sedimentation performance, and had positive industrial application prospects.

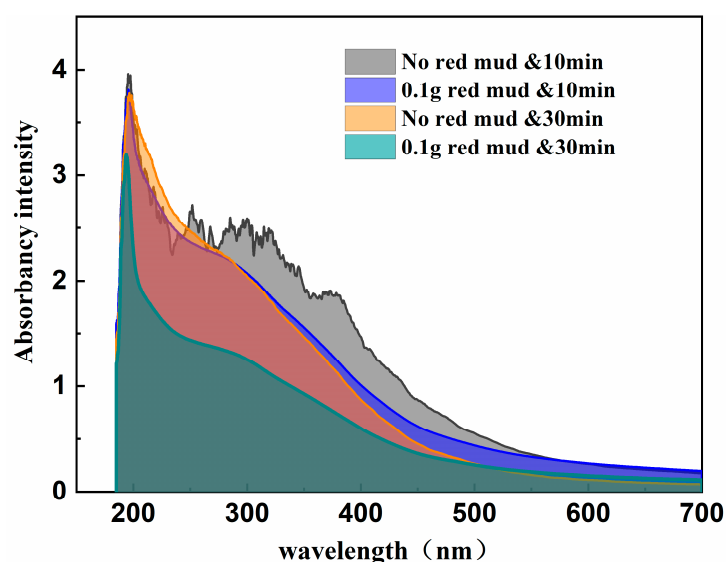


Figure 5. Ultraviolet spectrum of the supernatant in the sedimentation experiment.

3.3. Characterization of Red Mud and Arsenic Removal Residues

As shown in Figure 6, the XRD pattern of the arsenic removal residues produced in the arsenic removal experiments cannot indicate the presence of ferric arsenite in the arsenic removal residues because ferric arsenite is amorphous in structure. In Table 3, X-ray fluorescence spectrometry analysis of the original red mud shows that the red mud mainly contains elements such as oxygen, iron, aluminum, sodium, silicon, titanium, and calcium, and a large amount of arsenic is enriched in the arsenic removal residues.

Table 3. Analysis results of main chemical elements of the arsenic removal residues (%).

Element	O	Na	Al	Si	P	S	Ti	Fe	As
arsenic removal residues	26.87	0.93	3.85	2.62	0.05	0.24	1.75	41.61	21.45

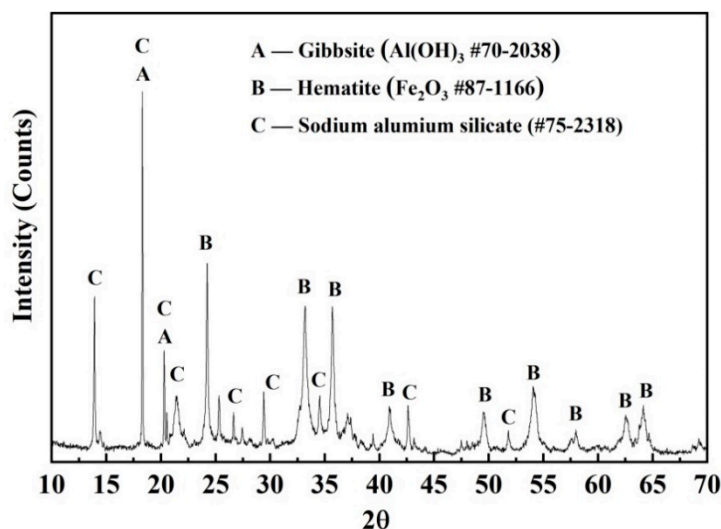


Figure 6. XRD of the arsenic removal residues.

The original red mud and arsenic removal residues were analyzed by XPS. The analysis objects were As3d, Fe2p, O1s, C1s, and the carbon element was used as the background to eliminate the error. The results are shown in Figures 7–10, and Table 4. The As3d, Fe2p, O1s peaks were deconvoluted, and the corresponding curve-fitting parameters are summarized in Table 5.

According to Figure 7, in the specific binding energy interval, the original red mud shows no arsenic peak, while the peak of the arsenic appeared in the arsenic removal residues with the binding energy at 44.39 eV and the peak value at 7736.29. Comparing with the standard arsenic peak, it was found that the arsenic ions on the surface of the arsenic removal residues mainly exist in the form of III valence. In Table 4, the original red mud contains a large amount of element such as oxygen, carbon, and iron, while a large amount of arsenic was found in the arsenic removal residues.

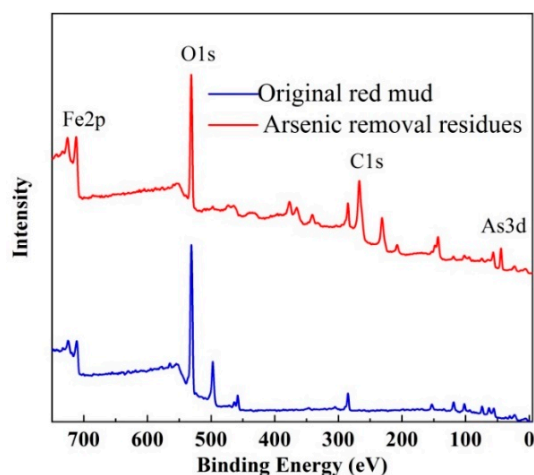


Figure 7. XPS spectrum of the original red mud/ arsenic removal residues.

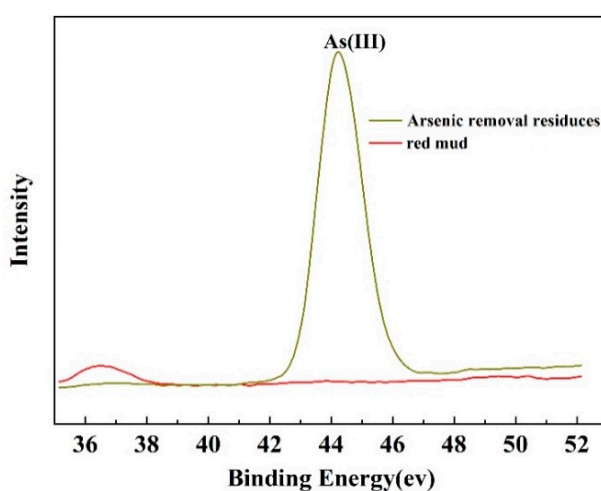
Table 4. XPS element analysis results.

Name	Original Red Mud		Arsenic Removal Residues	
	Peak BE (eV)	Atomic (%)	Peak BE (eV)	Atomic (%)
C1s	284.8	20.28	284.8	22.71
O1s	531.18	70.76	530.9	52.41
Fe2p	710.6	8.96	711.51	14.76
As3d	-	-	44.39	10.11

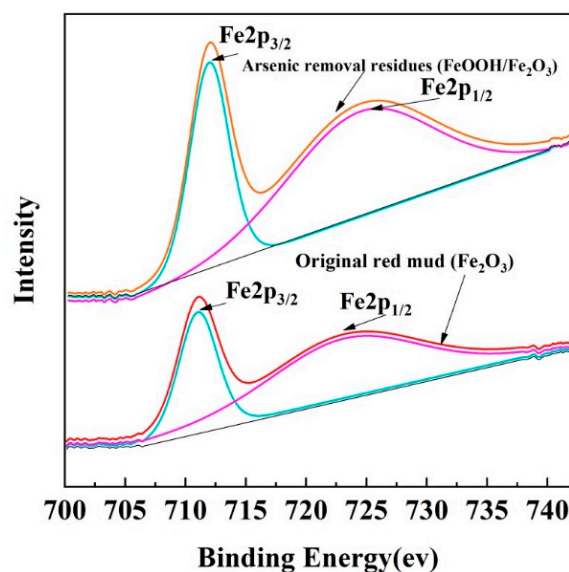
Table 5. XPS peak parameters for Fe 2p, As 3d, O1s spectra [33,34].

Spectral Peak	Binding Energy (eV)	FWHM	Chemical States
Fe 2p _{3/2}	711.98	3.85	FeOOH
Fe 2p _{3/2}	711.04	3.78	Fe ₂ O ₃
Fe 2p _{1/2}	724.51	14.60	FeOOH
Fe 2p _{1/2}	723.22	14.72	Fe ₂ O ₃
As 3d _{5/2}	44.39	1.67	As(III)–O
O 1s	529.5	1.25/0.7	Lattice oxygen (O ²⁻)
O 1s	531.2	1.62/2.15	Hydroxyl oxygen (OH ⁻)
O 1s	532.9	1.50	Attached water (H ₂ O)

The XPS spectra of As3d peaks of arsenic removal residues, ranged from 42.02 to 47.37 eV (Figure 8) and the peak was located at 44.39 eV, which indicated that the valence state of As in arsenic removal residues is +3 [35].

**Figure 8.** As3d spectrum chart of the arsenic removal residues.

According to Figure 9, at specific binding energy intervals, the peak value of iron ions in the arsenic removal residues is significantly higher than that of the original red mud, which resulted from the addition of a large amount of ferric iron to the test. Through comparative analysis, it was found that the peak of iron ions had shifted.

**Figure 9.** Fe2p spectrum chart of the original red mud and the arsenic removal residues.

The XPS spectra of O1s peaks of red mud and arsenic removal residues are provided in Figure 10. The binding energy of O1s of red mud at 529.5, 531.2, and 532.9 eV was mainly associated with O^{2-} in oxide phases, OH^- in hydroxide species, and oxygen in water, respectively [36,37]. It can be found that the XPS peak of oxygen ions in the arsenic removal residues shifted significantly. We can infer that the increase of hydroxide species on the surface could contribute to the generation of ferric hydroxide.

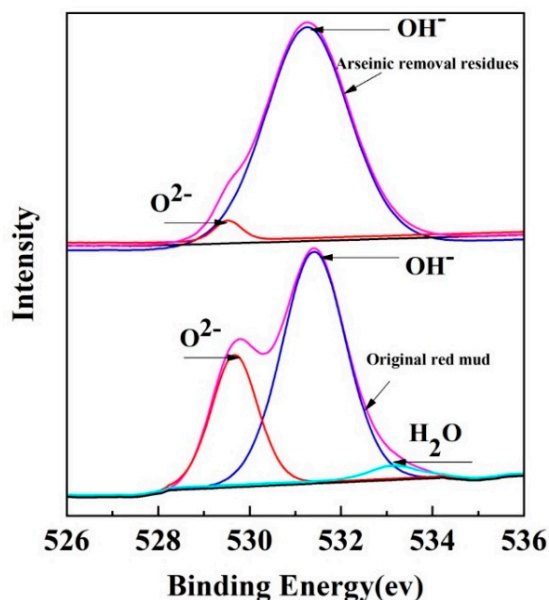


Figure 10. O1s spectrum chart of the original red mud and the arsenic removal residues.

The Raman spectra of the original red mud and arsenic removal residues (Figure 11) show that the Raman peak of iron ions is significantly enhanced, confirming the formation of $Fe_{1-x}(As)_x(OH)_3$ which attached on the red mud surface. At the same time, a new wide Raman band appeared at 803 cm^{-1} in the arsenic removal residues, which can be attributed to the stretching vibration of the As–O bands, which also confirms that ferric arsenite was formed [24]. It appears that the arsenic ion is separated from the solution by generating $Fe_{1-x}(As)_x(OH)_3$ on the red mud surface.

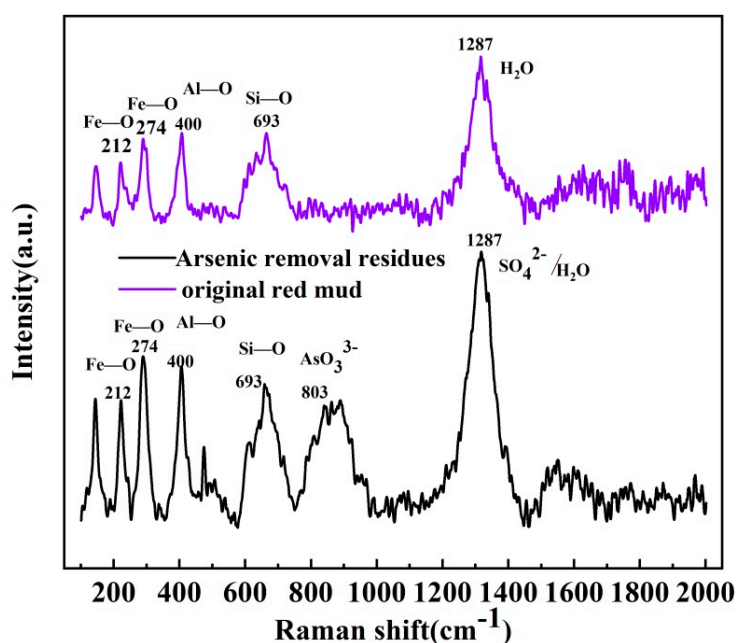


Figure 11. Raman spectrum of the original red mud/arsenic removal residues.

As shown in Figure 12, in the SEM images with magnification of 1000, the original red mud is dispersed as fine particles with a relatively uniform particle size, whereas agglomerated amorphous particles appear in the arsenic removal residues. In the image with a magnification of 10,000, the particles in the original red mud are more dispersed, and the fine-grained particles tend to aggregate together. Whereas the particles in the arsenic removal residues are large, there are some smaller amorphous substances attached on the surface of those large particles, which verifies the formation of amorphous $\text{Fe}_{1-x}(\text{As})_x(\text{OH})_3$ on the red mud particles. It also demonstrates that the generation of red mud/ $\text{Fe}_{1-x}(\text{As})_x(\text{OH})_3$ enhances the agglomeration of particles.

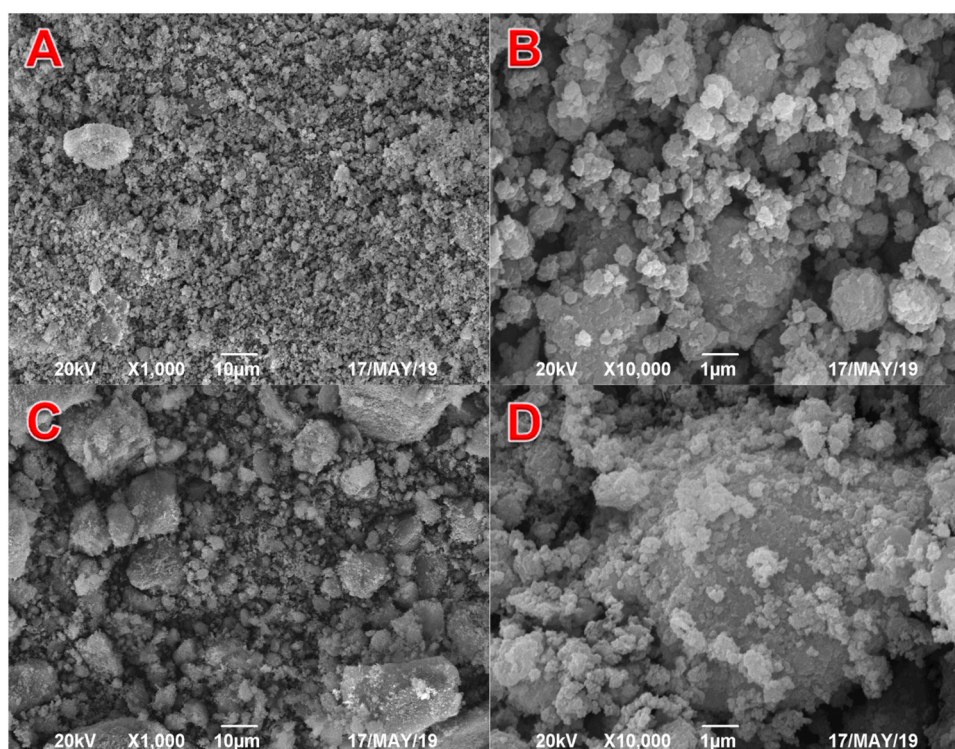


Figure 12. SEM of the solid surface before and after As removal (A,B—original red mud; C,D—arsenic removal residues).

4. Conclusion

Using red mud and ferric solution as raw materials, arsenic was efficiently removed from a high-concentration arsenic (III) solution by forming ferric arsenite on a red mud surface. At the Fe/As molar ratio of 3, the removal efficiency of the arsenic ions at 500 mg/L reached 98%. The ferric arsenite was generated on the surface of red mud to form red mud/ $\text{Fe}_{1-x}(\text{As})_x(\text{OH})_3$, and it was further aggregated to larger particles, which improved the sedimentation performance of the arsenic removal residues. The red mud was mainly used as the carrier of the arsenic removal residues. Additionally, both the alkalinity of red mud and the adsorption of arsenic on its surface played a role in the process.

Author Contributions: T.Y. and R.L. designed and supervised the project; Y.X. performed the experiments; D.H. and T.Y. analyzed the data and wrote this paper; L.W. and W.S. corrected it. All authors have read and agreed to the published version of the manuscript.

Funding: This work was supported by the National Key Scientific Research Project (2019YFC0408305), National 111 Project (No. B14034), The Collaborative Innovation Center for Clean and Efficient Utilization of Strategic Metal Mineral Resources, Key Laboratory of Hunan Province for Clean and Efficient Utilization of Strategic Calcium-Containing Mineral Resources (No. 2018TP1002).

Conflicts of Interest: The authors declare no conflict of interest.

References

1. Luong, V.T.; Canas Kurz, E.E.; Hellriegel, U.; Luu, T.L.; Hoinkis, J.; Bundschuh, J. Iron-based subsurface arsenic removal technologies by aeration: A review of the current state and future prospects. *Water Res.* **2018**, *133*, 110–122.
2. Nidheesh, P.V.; Singh, T.S.A. Arsenic removal by electrocoagulation process: Recent trends and removal mechanism. *Chemosphere* **2017**, *181*, 418–432.
3. Sarkar, A.; Paul, B. The global menace of arsenic and its conventional remediation—A critical review. *Chemosphere* **2017**, *173*, 630–631.
4. Sandoval, M.A.; Fuentes, R.; Nava, J.L.; Coreño, O.; Li, Y.; Hernández, J.H. Simultaneous removal of fluoride and arsenic from groundwater by electrocoagulation using a filter-press flow reactor with a three-cell stack. *Sep. Purif. Technol.* **2019**, *208*, 208–216.
5. Sanjrani, M.A.; Zhou, B.; Zhao, H.; Bhutto, S.A.; Muneer, A.S.; Xia, S.B. Arsenic contaminated groundwater in china and its treatment options, a review. *Appl. Ecol. Environ. Res.* **2019**, *17*, 1655–1683.
6. Zhang, Y.; Zhao, H.; Zhang, Y.; Liu, H.; Yin, H.; Deng, J.; Qiu, G. Interaction mechanism between marmatite and chalcocite in acidic (microbial) environments. *Hydrometallurgy* **2020**, *191*, 105217.
7. Tabelin, C.B.; Igarashi, T.; Villacorte-Tabelin, M.; Park, I.; Opiso, E.M.; Ito, M.; Hiroyoshi, N. Arsenic, selenium, boron, lead, cadmium, copper, and zinc in naturally contaminated rocks: A review of their sources, modes of enrichment, mechanisms of release, and mitigation strategies. *Sci. Total Environ.* **2018**, *645*, 1522–1553.
8. Luukkonen, T.; Runtti, H.; Niskanen, M.; Tolonen, E.T.; Sarkkinen, M.; Kemppainen, K.; Ramo, J.; Lassi, U. Simultaneous removal of Ni(II), As(III), and Sb(III) from spiked mine effluent with metakaolin and blast-furnace-slag geopolymers. *J. Environ. Manag.* **2016**, *166*, 579–588.
9. Kobya, M.; Gebologlu, U.; Ulu, F.; Oncel, S.; Demirbas, E. Removal of arsenic from drinking water by the electrocoagulation using Fe and Al electrodes. *Electrochim. Acta* **2011**, *56*, 5060–5070.
10. Dutta, P.K.P.S.O.; Sharma, V.K. Photocatalytic oxidation of arsenic (III): Evidence of hydroxyl radicals. *Environ. Sci. Technol.* **2005**, *39*, 1827–1834.
11. Leupin, O.X.; Hug, S.J. Oxidation and removal of arsenic (III) from aerated groundwater by filtration through sand and zero-valent iron. *Water Res.* **2005**, *39*, 1729–1740.
12. Gallagher, P.A.S.C.A.; Parks, A. Preservation of As (III) and As (V) in drinking water supply samples from across the united states using EDTA and acetic acid as a means of minimizing iron-arsenic coprecipitation. *Environ. Sci. Technol.* **2004**, *38*, 2919–2927.
13. Wang, H.-J.; Gong, W.-X.; Liu, R.-P.; Liu, H.-J.; Qu, J.-H. Treatment of high arsenic content wastewater by a combined physical–chemical process. *Colloids Surf. A Physicochem. Eng. Asp.* **2011**, *379*, 116–120.
14. He, Z.; Tian, S.; Ning, P. Adsorption of arsenate and arsenite from aqueous solutions by cerium-loaded cation exchange resin. *J. Rare Earths* **2012**, *30*, 563–572.
15. Kim, J.; Benjamin, M.M. Modeling a novel ion exchange process for arsenic and nitrate removal. *Water Res.* **2004**, *38*, 2053–2062.
16. Sabbatini, P.; Yrazu, F.; Rossi, F.; Thern, G.; Marajofsky, A.; Fidalgo de Cortalezzi, M.M. Fabrication and characterization of iron oxide ceramic membranes for arsenic removal. *Water Res.* **2010**, *44*, 5702–5712.
17. Yu, Y.; Zhao, C.; Wang, Y.; Fan, W.; Luan, Z. Effects of ion concentration and natural organic matter on arsenic(V) removal by nanofiltration under different transmembrane pressures. *J. Environ. Sci.* **2013**, *25*, 302–307.
18. Gallegos-Garcia, M.; Ramírez-Muñiz, K.; Song, S. Arsenic removal from water by adsorption using iron oxide minerals as adsorbents: A review. *Miner. Process. Extr. Metall. Rev.* **2012**, *33*, 301–315.
19. Guan, X.; Du, J.; Meng, X.; Sun, Y.; Sun, B.; Hu, Q. Application of titanium dioxide in arsenic removal from water: A review. *J. Hazard Mater.* **2012**, *215–216*, 1–16.
20. Mohan, D.; Pittman, C.U., Jr. Arsenic removal from water/wastewater using adsorbents—A critical review. *J. Hazard Mater.* **2007**, *142*, 1–53.
21. Srivastava, P.K.; Vaish, A.; Dwivedi, S.; Chakrabarty, D.; Singh, N.; Tripathi, R.D. Biological removal of arsenic pollution by soil fungi. *Sci. Total Environ.* **2011**, *409*, 2430–2442.
22. Niazi, N.K.; Bibi, I.; Shahid, M.; Ok, Y.S.; Burton, E.D.; Wang, H.; Shaheen, S.M.; Rinklebe, J.; Luttge, A. Arsenic removal by perilla leaf biochar in aqueous solutions and groundwater: An integrated spectroscopic and microscopic examination. *Environ. Pollut.* **2018**, *232*, 31–41.

23. Nazari, A.M.; Radzinski, R.; Ghahreman, A. Review of arsenic metallurgy: Treatment of arsenical minerals and the immobilization of arsenic. *Hydrometallurgy* **2017**, *174*, 258–281.
24. Yue, T.; Niu, Z.; Hu, Y.; Han, H.; Sun, W.; Tian, J.; Xu, Z.; Wang, L.; Yang, Y. Arsenic(V) adsorption on ferric oxyhydroxide gel at high alkalinity for securely recycling of arsenic-bearing copper slag. *Appl. Surf. Sci.* **2019**, *478*, 213–220.
25. Nikbin, I.M.; Aliaghazadeh, M.; Charkhtab, S.H.; Fathollahpour, A. Environmental impacts and mechanical properties of lightweight concrete containing bauxite residue (red mud). *J. Clean. Prod.* **2018**, *172*, 2683–2694.
26. Tabelin, C.B.; Corpuz, R.D.; Igarashi, T.; Villacorte-Tabelin, M.; Alorro, R.D.; Yoo, K.; Raval, S.; Ito, M.; Hiroyoshi, N. Acid mine drainage formation and arsenic mobility under strongly acidic conditions: Importance of soluble phases, iron oxyhydroxides/oxides and nature of oxidation layer on pyrite. *J. Hazard. Mater.* **2020**, *399*, 122844.
27. Bhatnagar, A.; Vilar, V.J.; Botelho, C.M.; Boaventura, R.A. A review of the use of red mud as adsorbent for the removal of toxic pollutants from water and wastewater. *Environ. Technol.* **2011**, *32*, 231–249.
28. Li, N.S.Z.M.; Run, F.H.; Du, D.Y. The mechanism of arsenic (III) removal by ferric chloride. *CIESC J.* **2012**, *63*, 2224–2205.
29. Chaudhry, S.I.S.S.A. Iron oxide and its modified forms as an adsorbent for arsenic removal: A comprehensive recent advancement. *Process Saf. Environ. Prot.* **2017**, *111*, 592–626.
30. Demopoulos, D.F.G.P. Arsenic immobilization by controlled scorodite precipitation. *JOM* **1997**, *49*, 52–55.
31. Donald Langmuir, J.M.; Anjali Macdonald, J.R. Predicting arsenic concentrations in the porewaters of buried uranium mill tailings. *Geochim. Cosmochim. Acta* **1999**, *63*, 3379–3394.
32. Langmuir, D.; Mahoney, J.; Rowson, J. Solubility products of amorphous ferric arsenate and crystalline scorodite ($\text{FeAsO}_4 \cdot 2\text{H}_2\text{O}$) and their application to arsenic behavior in buried mine tailings. *Geochim. Cosmochim. Acta* **2006**, *70*, 2942–2956.
33. Park, I.; Tabelin, C.B.; Seno, K.; Jeon, S.; Inano, H.; Ito, M.; Hiroyoshi, N. Carrier-microencapsulation of arsenopyrite using al-catechol complex: Nature of oxidation products, effects on anodic and cathodic reactions, and coating stability under simulated weathering conditions. *Heliyon* **2020**, *6*, e03189.
34. Wei, Y.; Liao, A.; Wang, L.; Wang, X.; Wang, D.; Zhou, Y.; Zou, Z. Room temperature surface modification of ultrathin FeOOH cocatalysts on Fe_2O_3 photoanodes for high photoelectrochemical water splitting. *J. Nanomater.* **2020**, *2020*, 1–7.
35. Liu, J.; Deng, S.; Zhao, F.; Cheng, H.; Frost, R.L. Spectroscopic characterization and solubility investigation on the effects of As(V) on mineral structure toeleite ($\text{Fe}_6(\text{AsO}_3)_2\text{SO}_4(\text{OH})_2 \cdot \text{H}_2\text{O}$). *Spectrochim. Acta A Mol. Biomol. Spectrosc.* **2015**, *134*, 428–433.
36. Ghahremaninezhad, A.; Dixon, D.G.; Asselin, E. Electrochemical and xps analysis of chalcopyrite (CuFeS_2) dissolution in sulfuric acid solution. *Electrochim. Acta* **2013**, *87*, 97–112.
37. Zhao, H.; Zhang, Y.; Sun, M.; Ou, P.; Zhang, Y.; Liao, R.; Qiu, G. Catalytic mechanism of silver in the oxidative dissolution process of chalcopyrite: Experiment and dft calculation. *Hydrometallurgy* **2019**, *187*, 18–29.

